N O T I C E

THIS DOCUMENT HAS BEEN REPRODUCED FROM MICROFICHE. ALTHOUGH IT IS RECOGNIZED THAT CERTAIN PORTIONS ARE ILLEGIBLE, IT IS BEING RELEASED IN THE INTEREST OF MAKING AVAILABLE AS MUCH INFORMATION AS POSSIBLE

NASA Technical Memorandum 79294

(NASA-TM-79294) DYNAMIC ANALYSIS OF NONCONTACTING FACE SEALS (NASA) 40 p HC A03/MF A01 CSCL 11A

N80-27695

Unclas
G3/37 27986

DYNAMIC ANALYSIS OF NONCONTACTING FACE SEALS

I. Etsion
Lewis Research Center
Cleveland, Ohio

May 1980

NASA

DYNAMIC ANALYSIS OF NONCONTACTING FACE SEALS

by I. Etsion

ABSTRACT

The dynamic behavior of a noncontacting coned face seal is analyzed taking into account various design parameters and operating conditions. The primary seal ring motion is expressed by a set of nonlinear equations for three degrees of freedom. These equations, which are solved numerically, allow identification of two dimensionless groups of parameters that affect the seal dynamic behavior. Stability maps for various seals are presented. These maps contain a stable-to-unstable transition region in which the ring wobbles at half the shaft frequency. The effect of various parameters on seal stability is discussed and an empirical expression for critical stability is offered.

E-458

NOMENCLATURE

A	$(1 - R)/H_m H^2(1 - R_i)$
a	linearity constant, eq. (38)
B	seal balance ratio, $(r_o^2 - r_b^2)/(r_o^2 - r_i^2)$
C	seal center-line clearance
C_o	equilibrium center-line clearance
F*	axial force
F_c^*	closing force
F_{spi}^*	initial spring load
F	dimensionless force, F/Sr_o^2
H	dimensionless film thickness, h/C
H_{min}	dimensionless minimum film thickness
h	film thickness
I*	ring mass moment of inertia about a diameter
I	dimensionless moment of inertia, $I^*\omega^2 C_o/Sr_o^4$
K*	spring constant
K	dimensionless spring constant, K^*/Sr_o
M*	moment
M_e^*	external moment
M	dimensionless moment, M/Sr_o^3
m*	ring mass
m	dimensionless mass, $m^*\omega^2 C_o/Sr_o^2$
n	number of seal revolutions
P	dimensionless pressure, p/S
p	pressure

R	dimensionless radius, r/r_o
r	radial coordinate
r_b	seal balance radius
r_g	ring radius of gyration
S	seal parameter, $6\mu\omega(r_o/C_o)^2 (1 - R_i)^2$
t^*	time
t	dimensionless time, ωt^*
Z^*	axial displacement
Z	dimensionless displacement, Z^*/C_o
α^*	tilt angle
α	normalized tilt, $\alpha^* r_o/C_o$
β^*	coning angle
β	normalized coning, $\beta^* r_o/C_o$
γ^*	nutation
γ	normalized nutation, $\gamma^* r_o/C_o$
δ	coning parameter, $\beta^* r_o/C$
ϵ	tilt parameter, $\gamma^* r_o/C$
θ	angular coordinate
μ	viscosity
ψ	precession
ω	shaft angular velocity

Subscripts:

1, 2, 3	axes 1, 2, or 3, respectively
d	hydrodynamic
i	inner radius
m	mid radius
o	outer radius

s	hydrostatic
sp	springs
x, y, z	axes, x, y, or z, respectively

INTRODUCTION

The presence of a fluid film between the mating faces of the primary seal ring and seal seat in a mechanical face seal (fig. 1) was established in the early 1960's by Denny [1]. Since then several different mechanisms which provide sources of fluid film load support have been proposed. These mechanisms include surface waviness, angular misalinement, thermal and mechanical distortions, and phase change. The state of the art is well summarized in reference [2] and some of the latest results on seal theory are presented in references [3 - 9]. From all these works it is evident that the pressure developed in the lubricating film is strongly dependent on the shape and magnitude of the film thickness between the mating faces. Almost all the analyses published so far assume a given fixed shape of the film thickness and then calculate the resulting pressure distribution from which forces, moments, flow rates, and friction can be derived. In reality, however, the elements forming the seal are not rigidly mounted. Hence, the film thickness is both space and time dependent.

The main objective in any seal is to minimize leakage. To this end the separation of the mating faces should be as small as possible. However, too small a clearance increases friction losses and can result in excessive wear. Therefore a proper sealing gap has to be maintained at all times to ensure safe and reliable operation. Short life, due to surface damage, and excessive

leakage are common problems in face seals. These problems can be attributed to unstable operation which causes variations of the sealing gap beyond permissible limits. Indeed, dynamic instability in the form of vibration of flexibly mounted elements was experimentally observed in face type seals [10 - 14].

The primary seal ring in a face seal (fig. 1) is flexibly mounted so that only its circumferential rotation is prevented. Hence, the ring has five degrees of freedom; axial displacement, two angular tilts about two orthogonal diameters, and two perpendicular radial displacements. Such a system can be vulnerable to several sources of instabilities which are discussed in the seal literature mentioned above. In order to avoid unstable operation a mechanical face seal has to be designed with a great care regarding the mass, inertia, stiffness, and damping combinations for selected geometries and operation conditions. To this end a complete dynamic analysis is required which takes into account the various parameters affecting seal stability.

Only a few attempts have been made so far to analyze seal dynamics. Most of these analyses deal with only one degree of freedom or overlook some or all of the fluid film effects [15 - 19]. A proper treatment of the problem is presented in reference [20] but it treats a special case where the system forces and moments are provided by a supporting gas bearing and not by the sealing dam. In more recent work [21, 22] the motion of a flexibly mounted ring in a noncontacting face seal is described in its three major degrees of freedom (one axial and two angular). Hydro-

dynamic, hydrostatic, and squeeze film effects as well as the contribution of the flexible support to the system dynamics are considered and it is shown how the seal stability is affected by various design parameters. The analysis in references [21] and [22] is, however, somewhat limited in that it is based on small perturbation in the seal clearance and assumes flat faces.

The objective of this paper is to present a more comprehensive dynamic analysis of a noncontacting face seal. The nonlinear equations of motion of the primary seal ring in its major three degrees of freedom are solved numerically, giving the complete transient behavior of the ring. In addition, coning of the mating faces is included, thus, resulting in a more realistic model in which balance ratio and initial spring loading are also considered.

THEORY

The theoretical model is shown in figure 2. The seal seat is parallel to the plane xy of an inertial reference xyz and is rotating at a constant angular velocity ω about the z axis. The primary seal ring has three degrees of freedom, it can move axially along the z axis and tilt about the x and y axes. A rotating coordinate system 123 coincides with the principal axes of the ring so that axis 3 is perpendicular to the plane of the ring. The coordinate system 123 rotates in the inertial reference xyz so that axis 1 always remains in the plane xy and axis 2 is directed to the instantaneous point of maximum film thickness. Thus, the orientation of coordinate system 123 in the inertial reference xyz can be defined by the nutation angle γ^* measured from axis z to axis 3, and the precession angle ψ measured from axis x to axis 1.

Due to the tiny clearance C (of the order of few micrometers in typical seals) the nutation angle γ^* is also very small. Hence, as shown in [21] the equations of motion of the seal ring are

$$F_z^* = m^* \ddot{Z} \tag{1}$$

$$M_x^* = I^* \ddot{\alpha}_x \tag{2}$$

$$M_y^* = I^* \ddot{\alpha}_y \tag{3}$$

where $\ddot{\alpha}_x^*$ and $\ddot{\alpha}_y^*$ represent the acceleration of the ring about the x and y axes, respectively.

The system of force F_z^* and moments M_x^* and M_y^* is composed of fluid film pressures, pressure from mechanical springs, and sealed pressure on the back of the ring. The moments acting on the ring are more readily obtained with respect to axes 1 and 2 of the rotating coordinate system 123 and then transformed into the inertial reference xyz. This transformation takes the form of (see fig. 3)

$$M_x^* = M_1^* \cos \psi - M_2^* \sin \psi \tag{4}$$

$$M_y^* = M_1^* \sin \psi + M_2^* \cos \psi \tag{5}$$

The moment M_3^* contributes the terms $M_3^* \sin \gamma^* \sin \psi$ and $-M_3^* \sin \gamma^* \cos \psi$ to M_x^* and M_y^*, respectively. However, using Euler's equations of motion it can be shown that for $\gamma^* << 1$, which is our case, M_3^* itself is of order γ^{*2} and therefore can be neglected.

The moments M_1^* and M_2^* are calculated from

$$M_1^* = \int_0^{2\pi} \int_{r_i}^{r_o} pr^2 \cos\theta \, dr \, d\theta - M_{sp}^* \tag{6}$$

$$M_2^* = \int_0^{2\pi} \int_{r_i}^{r_o} pr^2 \sin\theta \, dr \, d\theta \tag{7}$$

and the force F_z^* is

$$F_z^* = \int_0^{2\pi} \int_{r_i}^{r_o} pr \, dr \, d\theta - F_c^* \tag{8}$$

where M_{sp}^* is the restoring moment provided by the flexible support (e.g., mechanical springs) and F_e^* is a closing force contributed by both the flexible support and the pressure balance of the seal (see appendix 1).

The pressure distribution, p, is found from a solution of the Reynolds equation which, by using the narrow seal approximation [23], reduces to

$$\frac{\partial}{\partial r}\left(h^3 \frac{\partial p}{\partial r}\right) = 6\mu \left(\omega \frac{\partial h}{\partial \theta} + 2 \frac{\partial h}{\partial t^*}\right) \tag{9}$$

The boundary conditions of equation (9) are

$p = p_i$ at $r = r_i$

$p = p_o$ at $r = r_o$

Because of its linear nature, equation (9) can be solved separately for the

hydrostatic, hydrodynamic, and squeeze components of the pressure [6, 7, 8]. The hydrostatic pressure component is

$$p_s = p_o - (p_o - p_i)\frac{h_i^2}{h_o^2 - h_i^2}\left[\left(\frac{h_o}{h}\right)^2 - 1\right] \tag{10}$$

The hydrodynamic and squeeze pressure components can be combined to give

$$p_d = -3\mu\left(\omega\frac{\partial h}{\partial \theta} + 2\frac{\partial h}{\partial t^*}\right)\frac{(r_o - r)(r - r_i)}{h_m h^2} \tag{11}$$

and the total pressure is the sum of p_s and p_d. Hence, the complete solution of equation (9) is

$$p = p_s + p_d \tag{12}$$

Assuming that the mating faces have some coning β^* which can result from either thermal and mechanical distortion, or can be intentionally machined into one of the surfaces, the film thickness distribution h is (see fig. 2)

$$h = C + \gamma^* r \cos\theta + \beta^*(r - r_i) \tag{13}$$

Visualizing an angle φ measured from the y axis to a plane defined by the z axis and a point (r, θ) on the ring face (fig. 2), we have for $\gamma^* \ll 1$

$$\theta = \varphi - \psi \tag{14}$$

where φ is fixed in time. Hence, substituting (14) in (13), differentiating

and neglecting curvature effects we have

$$\frac{\partial h}{\partial \theta} = -\gamma^* r_m \sin\theta \tag{15}$$

and

$$\frac{\partial h}{\partial t^*} = \dot{Z}^* + \dot{\gamma}^* r_m \cos\theta + \dot{\psi}\gamma^* r_m \sin\theta \tag{16}$$

where the dots indicate differentiation with respect to time.

Using the normalized parameters $\gamma = \gamma^* r_o/C_o$, $R = r/r_o$, $t = \omega t^*$, and $Z = Z^*/C_o$ where C_o is the designed clearance (see appendix 2). Noting that

$$C = C_o + Z^* = C_o(1 + Z)$$

and normalizing the film thickness in the form

$$H = \frac{h}{C} = 1 + \epsilon R \cos\theta + \delta(R - R_i) \tag{17}$$

we have, from equations (10) and (11),

$$P_s = P_o - (P_o - P_i)H_i^2(H_o + H)\frac{A}{2} \tag{18}$$

$$P_d = \left[\left(\frac{1}{2} - \dot{\psi}\right)\gamma R_m \sin\theta - \dot{Z} - \gamma R_m \cos\theta\right]\frac{A}{(1 + Z)^3}\frac{R - R_i}{1 - R_i} \tag{19}$$

In equations (18) and (19) A is simply

$$A = \frac{1 - R}{H_m H^2 (1 - R_i)} \tag{20}$$

and P is a dimensionless pressure obtained from $P = p/S$. The term S is a seal parameter having dimension of pressure and defined as

$$S = 6 \mu\omega \left(\frac{r_o}{C_o}\right)^2 (1 - R_i)^2 \tag{21}$$

Using the seal parameter S to normalize forces and moments in the form $F = F^*/Sr_o^2$ and $M = M^*/Sr_o^3$, recalling the normalized time t and axial displacement Z, and using a normalized tilt in the form $\alpha = \alpha^* r_o/C_o$, the equations of motion (1), (2), and (3) become

$$F_z = m\ddot{Z} \tag{22}$$

$$M_x = I\ddot{\alpha}_x \tag{23}$$

$$M_y = I\ddot{\alpha}_y \tag{24}$$

Equations (22) to (24) can be solved for the accelerations from which the ring motion can be found.

NUMERICAL CALCULATION

In order to examine the dynamic behavior of the seal the flexibly mounted ring is disturbed from its equilibrium position $\gamma = \dot{\gamma} = 0$, $Z = \dot{Z} = 0$. The new tilt and coning parameters ϵ and δ are calculated from

$$\epsilon = \gamma^* \frac{r_o}{C} = \frac{\gamma}{1 + Z} \tag{25}$$

$$\delta = \beta^* \frac{r_o}{C} = \frac{\beta}{1 + Z} \tag{26}$$

These parameters are used in equations (17) and (20) to find the film thickness distribution H and the parameter A, respectively. The ring area is divided radially and circumferentially by a fine grid and the pressures P_s and P_d are calculated at each grid point using equations (18) and (19). The total pressure P is then calculated at each point by adding P_s and P_d, hence,

$$P = P_s + P_d \tag{27}$$

Any negative value of the total pressure P is replaced by $P = 0$, thereby taking account of possible cavitation. The discrete pressures are then integrated numerically to obtain the fluid film force and moments with the cavitation effect included. Hence, from equations (6), (7), and (8),

$$M_1 = \int_0^{2\pi} \int_{R_i}^{1} PR^2 \cos\theta \, dR \, d\theta - M_{sp} \tag{28}$$

$$M_2 = \int_0^{2\pi} \int_{R_i}^{1} PR^2 \sin\theta \, dR \, d\theta \tag{29}$$

$$F_z = \int_0^{2\pi} \int_{R_i}^{1} PR \, dR \, d\theta - F_c \tag{30}$$

The moments M_1 and M_2 are used to calculate M_x and M_y by equations (4) and (5) and the accelerations $\ddot{Z}$, $\ddot{\alpha}_x$, and $\ddot{\alpha}_y$ are calculated from equations (22), (23), and (24). The new velocities $\dot{Z}$, $\dot{\alpha}_x$, and $\dot{\alpha}_y$ and new displacements Z, α_x, and α_y are found by a time integration routine and the new nutation γ and precession ψ are calculated using the relations (see fig. 3)

$$\alpha_x = \gamma \cos \psi \tag{31}$$

$$\alpha_y = \gamma \sin \psi \tag{32}$$

which are valid for small angles. Differentiating equations (31) and (32) with respect to time we have

$$\dot{\alpha}_x = \dot{\gamma} \cos \psi - \gamma \dot{\psi} \sin \psi \tag{33}$$

$$\dot{\alpha}_y = \dot{\gamma} \sin \psi + \gamma \dot{\psi} \cos \psi \tag{34}$$

Hence, $\dot{\gamma}$ and $\dot{\psi}$ can be calculated from the already known $\dot{\alpha}_x$, $\dot{\alpha}_y$, γ, and ψ. A new film thickness H and pressure distribution P can now be found and the whole process is repeated.

The procedure described above is carried on in time giving the transient dynamics of the seal. At each time step the minimum film thickness is calculated and tested against a failure criterion. As can be seen from figure 2, contact can take place on either the inner or the outer radius of

the ring at $\theta = \pi$. Hence, by equation (17), the minimum film thickness is calculated from either

$$H_{min} = 1 - \epsilon R_i \tag{35}$$

or

$$H_{min} = 1 - \epsilon + \delta(1 - R_i) \tag{36}$$

whichever is smaller. The transient behavior of H_{min} serves as an indication of seal stability. Starting from the instant of the disturbance, H_{min} can decrease, increase, or reach a constant value. If H_{min} increases or reaches $H_{min} = \text{const}$ the seal is considered stable (with the special case of $H_{min} = 1$ for parallel operation). If, however, H_{min} is ever decreasing, and eventually diminishes, a face contact occurs and the seal is unstable.

RESULTS AND DISCUSSION

Three different values of seal radius ratio R_i were examined, these are: 0.8, 0.9, and 0.98. At each radius ratio a variety of design parameters and operation conditions were tested and three distinct modes of operation were identified. The data are presented in figures 4, 5, and 6 in the form of stability maps. An interesting and useful result is the relation found between the dimensionless groups of parameters $(r_g/r_{sp})^2 m^* \omega^2 / K^*$ and $(r_m/r_{sp})^2 (p_o - p_i) \times r_o^2 / K^* C_o$, where r_g is the ring radius of gyration relating mass and inertia by

$$I^* = \frac{1}{2} m^* r_g^2$$

From the many cases run on the computer, it was found that the critical sta-

bility, or the transition from stable to unstable mode of operation, is characterized by the expression

$$\left(\frac{r_g}{r_{sp}}\right)^2 \left(\frac{m^*\omega^2}{K^*}\right)_{cr} = 4 + a\,\frac{(p_o - p_i)r_o^2}{K^*C_o}\left(\frac{r_m}{r_{sp}}\right)^2 \tag{37}$$

with a as a linearity constant. Whenever $m^*\omega^2/K^*$ is less than the critical value $(m^*\omega^2/K^*)_{cr}$ given in equation (37), any disturbance of the ring from its equilibrium position vanishes after awhile and the seal is stable. When $m^*\omega^2/K^*$ is larger than the critical value, the seal becomes unstable, any disturbance increases in time causing eventual seal failure due to face contact. The transition from stable to unstable operation takes place in a narrow band adjacent to the critical value $(m^*\omega^2/K^*)_{cr}$ as is indictated by the shaded areas in figures 4 to 6. In this transition region the nutation γ^* and, hence, the minimum clearance, reach a constant value while the ring wobbles at half the shaft frequency.

The linearity constant, a, in equation (37) is a function of the radius ratio R_i and the normalized coning β. With the exception of the cases corresponding to $R_i = 0.8$ and $\beta < 5$, the constant a in all the other cases was found to be approximated fairly by

$$a = -8\pi R_i^2(1 - R_i)^2\,\frac{1 - \beta R_i}{\left[2 + \beta(1 - R_i)\right]^2} \tag{38}$$

This constant, which represents the slope of the stability threshold lines in figures 4 to 6, is maximized, as can be seen from equation (38), whenever the coning is

$$\beta_{opt} = \frac{2}{R_i(1 - R_i)} \tag{39}$$

Hence, at each radius ratio the stability region can be increased by increasing the normalized coning up to the optimum value of β_{opt}. Further increase of the normalized coning results in reducing the stability.

Ten representative cases at $R_i = 0.9$ were selected to demonstrate the various modes of seal behavior and the affect of various parameters on its stability. The characteristics of these cases are summarized in table I. Some of the computer program results are shown in figures 7 to 11, and the effects of various parameters are discussed below.

Dimensionless Group $(r_g/r_{sp})^2 m^* \omega^2/K^*$

The effect of values of the group of parameters $(r_g/r_{sp})^2 m^* \omega^2/K^*$ on seal stability is shown in figures 7, 8, and 9. Figure 7 presents time variation of the minimum clearance, H_{min}, vs. the number of seat revolutions after the ring is disturbed from its equilibrium. Figures 8 and 9 present the motion of the ring in its angular and axial degrees of freedom, respectively. Starting with figure 7 and using the stability map for $R_i = 0.9$ (fig. 5) we see that case 1 is in the unstable regime, case 2 in the transition region, and cases 3 and 4 are in the stable regime of operation. From figure 7 we see that in case 1, after the ring is slightly disturbed, the minimum clearance is slowly decreasing and after about 20 revolutions the seal fails due to face contact. The failure in case 1 is associated with increasing amplitude of angular vibrations as described by α_y in figure 8 and also an increase in the center-line clearance, C, as shown by the axial displacement in figure 9.

In case 2 the initial disturbance disappears rapidly, after about 1.5 revolutions. From there on the minimum clearance is maintained constant at $H_{min} = 0.51$ as shown in figure 7, while α_y (fig. 8) oscillates at a constant amplitude and at half the shaft speed. In the absence of an external moment the ring rotation about the x axis is identical to the one about the y axis with only a phase shift between the two motions. In the transition between stable and unstable modes of operation, represented by case 2, the phase shift is 90 degrees, hence, α_y and α_x result in a constant nutation γ and a constant precession $\dot{\psi} = \omega/2$. The axial displacement in case 2 (not shown) also maintains a constant value which is $Z = 0.145$. Thus, the center-line clearance is increased slightly due to the constant nutation γ.

Case 3 is a stable case with a rapid decay of any disturbance as shown in figures 7 and 8. Case 4 is similar to case 3 with the addition of an external moment M_e. As a result of the external moment, which can be caused, for example, by manufacturing tolerances in the supporting springs, the equilibrium position of the ring is not parallel to the seat. This can be seen from figure 7 where H_{min} reaches a constant value of 0.29 rather than 1.0 as in case 3. The ring remains tilted with respect to the seat, with α_x and α_y also maintaining constant values (not shown), and the center-line clearance increased by about 25 percent as shown in figure 9. The initial axial disturbance in case 4 was small compared to the angular one. However, the amplitude of the axial vibration is large during the first three revolutions as can be seen from figure 9. This could be a problem in cases where the ring is underdamped and the axial vibration decay slowly.

Normalized Coning $\beta^* r_o/C_o$

Figure 10 presents the effect of the normalized coning β on the seal behavior. Again from figure 5 we see that case 5, which corresponds to

$\beta = 2$, is in the unstable regime while cases 3, 6, and 7 are stable. Indeed, in figure 10 H_{min} for case 5 approaches zero while in the other three cases H_{min} approaches 1.0 (ring parallel to the seat). Comparing the three stable cases we see that case 3 with $\beta = 10$ is the most stable while case 7 with the relatively large coning $\beta = 100$ is the least stable. This result complies with the finding of an optimum coning which by equation (39) and for $R_i = 0.9$ is $\beta_{opt} = 22$. Increasing the coning above the optimum not only makes the seal less stable but also results in underdamping of the system. Case 7 is severely underdamped and as can be seen from figures 10, 8, and 9, the fluctuations in H_{min}, α_y, and Z persist much longer than in the other stable cases.

Dimensionless Group $(r_m/r_{sp})^2(p_o - p_i)r_o^2/K^*C_o$

Figure 11 shows the effect of the group of parameters $(r_m/r_{sp})^2(p_o - p_i)r_o^2/K^*C_o$. All the four cases compared in figure 11 correspond to a coning $\beta = 10$ and, as can be seen from figure 5, with the exception of case 1, are in the stable regime of operation. Thus, increasing the pressure differential, for example, can make an unstable seal to become stable. As shown in figure 11, this stabilization effect is associated with some underdamping but both the initial disturbance and the fluctuation in H_{min} die out very rapidly.

Radius Ratio r_i/r_o

The effect of R_i on stability is clearly presented by figures 4 to 6 from which it is seen that wider seals have larger range of stable operation. However, from equation (39) we see that for $R_i > 0.5$, which is the practical case, β_{opt} decreases as R_i decreases, and while for $R_i = 0.98$ β_{opt} is about 102, for $R_i = 0.8$ β_{opt} is only 12.5. This has an effect on the critical damping of the system. In trying to keep C_o as small as possible to reduce leakage, a wider seal may be operating with $\beta > \beta_{opt}$ and, hence, become underdamped and less stable.

From the results of the 10 representative cases shown in figures 7 to 11 we see that, in general, reducing the ring mass m^*, its radius of gyration r_g, and the operating speed ω have a stabilizing effect. Increasing the coning angle β^* or reducing the center-line clearance C_o stabilize the seal as long as the normalized coning $\beta^* r_o/C_o$ does not exceed the optimum coning β_{opt} given by equation (39). If the normalized coning β is too high, the system is underdamped and the range of stable operation is reduced. Increasing the pressure p_o on the outer diameter of the seal is beneficial from the stability standpoint although with increasing pressure the seal may again become underdamped. Increasing the spring constant K^* and spring location r_{sp} is also favorable for stable operation. An external moment, although not necessarily affecting the stability, results in a relative tilt between the ring and the seat associated with an increase in the center-line clearance C and reduction in minimum clearance H_{min}. This, in turn, increases the leakage across the sealing dam and can also make the minimum clearance dangerously small. A major source of external moment is an uneven spring support, hence, effort should be made to eliminate such source. This demand, combined with the requirement of stiffer springs for more stability, may call for a new approach in designing the flexible support for the seal ring.

The present analysis treats an ideal seal model in which the seat is perfectly aligned with the shaft, and in which secondary seal friction is neglected. In reality, some runout of the seat is almost unavoidable and friction cannot be totally eliminated. These two factors, however, do not alter the basic behavior of mechanical face seals, and the three modes of stable, transition, and unstable operation discussed in this work were experimentally observed

in cases where runout and friction do exist [24]. In reference [22] it is shown that the amount of runout does not affect the stability limits of the seal. Hence, a stable ring will synchronously track the misaligned rotating seat, an unstable ring will contact the seat because of increasing vibration, and in the transition region half frequency wobble is superimposed on the synchronous tracking motion of the ring. Friction may help in cases of underdamped systems but will not allow parallel tracking whenever runout exists. Parallel tracking is essential for minimum leakage and from this standpoint friction is undesirable and should be minimized.

CONCLUDING REMARKS

The dynamic behavior of a noncontacting face seal is analyzed taking into account various design parameters and operating conditions. The analysis is based on an analytical solution of the Reynolds equation for the fluid film pressure combined with a numerical solution, using time integration techniques, of the equations of motion of the flexibly mounted seal ring.

Three modes of seal operation are found that depend on two dimensionless groups of parameters. The seal can be either stable, unstable, or operate in a transition mode. In the stable regime any disturbance of the ring from its equilibrium position decays after awhile. In the unstable regime seal failure occurs due to face contact. In the transition region the ring wobbles with a constant amplitude at frequency that equals half the shaft speed.

Stability maps for several radius ratios are presented and the effect of various parameters on the dynamic behavior is demonstrated and discussed through some representative cases. An empirical expression for stability threshold of face seals is given along with an expression for optimum coning.

It is believed that the present approach will result in a better understanding of the mechanism of operation of mechanical face seals, and will enable the design of more predictable and reliable seals.

ACKNOWLEDGEMENT

The research reported here was performed while the author held a NRC-NASA research associateship at NASA Lewis Research Center, Cleveland, Ohio. Acknowledgement is also due Mr. B. Auer who programmed the analysis.

APPENDIX 1

CLOSING FORCE F_c AND RESTORING MOMENT M_{sp}

Considering only the support stiffness and neglecting friction due to the secondary seal and antirotation locks, the flexible support can be represented by a spring constant K^*. Assuming a continuous spring distribution the spring constant per unit of circumferential length is $K^*/2\pi r_{sp}$ where r_{sp} is the radius of springs location. Initially the ring is pressed against the seat by a spring preload F^*_{spi}. As the pressure differential is applied and the ring lifts off, the spring force, tending to close the sealing gap, increases to

$$F^*_{sp} = F^*_{spi} + K^*C \tag{40}$$

The spring force F^*_{sp} in equation (40) is not affected by the nutation γ^* (see fig. 2) since the additional compression of the springs over one half of the ring circumference is counter-balanced by equal relief of compression over the other half.

The total closing force is combined of the spring force F^*_{sp} and the outcome of the pressures acting on the back side of the ring. If r_b is the balance radius (the radius at which the secondary seal contacts the primary ring in fig. 1), then the total closing force is

$$F^*_c = F^*_{sp} + \pi\left(r_o^2 - r_b^2\right)p_o + \pi\left(r_b^2 - r_i^2\right)p_i$$

Using the seal balance ratio $B = \left(r_o^2 - r_b^2\right)\Big/\left(r_o^2 - r_i^2\right)$ the closing force is

$$F^*_c = F^*_{spi} + K^*C + \pi\left(r_o^2 - r_i^2\right)\left[p_oB + p_i(1 - B)\right] \tag{41}$$

The restoring moment generated by the support is not affected by axial displacement but by the nutation γ^* alone. Hence,

$$M^*_{sp} = \frac{K^*}{2\pi r_{sp}} \int_0^{2\pi} \gamma^* r^3_{sp} \cos^2\theta \; d\theta = \frac{K^*}{2} r^2_{sp} \gamma^* \tag{42}$$

Normalizing equations (41) and (42) the dimensionless force and moment are

$$F_c = F_{spi} + K \frac{C_o}{r_o} (1 + Z) + \pi \left(1 - R_i^2\right) \left[P_o B + P_i (1 - B)\right] \tag{43}$$

$$M_{sp} = \frac{K}{2} R^2_{sp} \gamma \frac{C_o}{r_o} \tag{44}$$

In the absence of an external moment the primary ring is balanced at $Z = \gamma = 0$ by the closing force F^*_c and the axial force generated by the fluid film pressure. From equation (19) it is clear that at equilibrium, $Z = \gamma = 0$, the pressure component $P_d = 0$. Hence, only the hydrostatic pressure P_s contributes to the fluid film axial force F^*. At equilibrium when $Z = 0$ we also have $\delta = \beta$ and the fluid film axial force is (ref. 6)

$$F^* = \pi r_m (r_o - r_i) \left[p_i + p_o + \frac{\beta(1 - R_i)}{2 + \beta(1 - R_i)} (p_o - p_i) \right] \tag{45}$$

Normalizing equation (45) and substituting for the closing force which corresponds to $Z = 0$ in equation (43), the closing force F_c becomes

$$F_c = K \frac{C_o}{r_o} Z + \pi R_m (1 - R_i) \left[P_i + P_o + \frac{\beta(1 - R_i)}{2 + \beta(1 - R_i)} (P_o - P_i) \right] \tag{46}$$

APPENDIX 2

THE DESIGNED CLEARANCE C_o AND BALANCE RATIO B

In analyzing noncontacting seal dynamics the design clearance C_o is to be known. It is used in the normalization of various parameters and is very important for leakage prediction.

Using the equilibrium fluid film axial force of equation (45), substituting $C = C_o$ in equation (41) and equating (41) and (45), noting that $r_o + r_i = 2r_m$, we have at equilibrium

$$F^*_{spi} + 2\pi r_m(r_o - r_i)\left(B - \frac{1}{2}\right)(p_o - p_i)$$

$$= \pi r_m(r_o - r_i)\frac{\beta(1 - R_i)}{2 + \beta(1 - R_i)}(p_o - p_i) - K^*C_o \qquad (47)$$

Hence, C_o can be found for any given set of the parameters F^*_{spi}, B, $(p_o - p_i)$, β^*, K^*, r_o, and r_i. Alternatively the equilibrium clearance C_o can be preselected from leakage consideration, for example, and other parameters like the initial spring load F^*_{spi}, or the balance ratio B, necessary to maintain the selected clearance can be calculated.

In noncontacting face seals the range of balance ratio values is limited by the normalized coning β. Dividing equation (47) by Sr_o^2 and rearranging we have

$$F_{spi} = \pi R_m(1 - R_i)(P_o - P_i)\left[\frac{\beta(1 - R_i)}{2 + \beta(1 - R_i)} - 2\left(B - \frac{1}{2}\right)\right] - K\frac{C_o}{r_o} \qquad (48)$$

For practical reasons the initial spring load F_{spi} has to be positive, hence, the right hand side of equation (48) must also be positive. Since the spring constant K is always positive, the balance ratio B will have an upper or lower limit depending on the magnitude of $(P_o - P_i)$. If $(P_o - P_i) > 0$ then B has an upper limit given by

$$B < \frac{1}{2}\left[1 + \frac{\beta(1 - R_i)}{2 + \beta(1 - R_i)}\right] \tag{49}$$

resulting in a balance ratio that is always less than 1.0. If, however, $(P_o - P_i) < 0$ then B has a lower limit given by

$$B > \frac{1}{2}\left[1 + \frac{\beta(1 - R_i)}{2 + \beta(1 - R_i)}\right] \tag{50}$$

which results in a balance ratio that is always larger than 0.5. Equation (48) with the requirement of $F_{spi} > 0$ along with the conditions (49) and (50) provide the range of balance ratio and spring constant values from which K* and B can be selected for a desired equilibrium clearance C_o. After K* and B are selected to meet these conditions, the required initial spring load can be calculated from (47).

It is worthwhile noticing that in noncontacting face seals, the required balance ratio B, as given by equations (49) and (50), may be negative when $p_o > p_i$, and may be larger than unity when $p_o < p_i$. The first case corresponds to $r_b > r_o$ while the second corresponds to $r_b < r_i$.

REFERENCES

1. Denny, D. F.: Some Measurements of Fluid Pressures Between Plane Parallel Thrust Surfaces With Special Reference to the Behaviour of Radial Face Seals. Wear, vol. 4, no. 1, Jan. 1961, pp. 64-83.

2. Ludwig, L. P.; and Greiner, H. P.: Designing Mechanical Face Seals for Improved Performance, Part 2 - Lubrication. Mech. Engrg., vol. 100, no. 12, Dec. 1978, pp. 18-23.

3. Nau, B. S.: Observation and Analysis of Mechanical Seal Film Characteristics. ASME paper 79-Lub-36 presented at the ASME-ASLE Lubrication Conf., Oct. 1979.

4. Lebeck, A. O.: A Mixed Friction Hydrostatic Face Seal Model with Phase Change. Jour. of Lub. Tech., Trans. ASME, Vol. 102, No. 2, April 1980, pp. 133-138.

5. Hughes, W. F.; and Cho, N. H.: Phase Change in Liquid Face Seals. II - Isothermal and Adiabatic Bounds with Real Fluids. ASME paper 79-Lub-6 presented at the ASME-ASLE Lubrication Conf., Oct. 1979.

6. Etsion, I.; and Sharoni, A.: Performance of End Face Seals with Diametral Tilt and Coning - Hydrostatic Effects. ASLE Trans., vol. 23, no. 3, July 1980, pp. 279-288.

7. Sharoni, A.; and Etsion, I.: Performance of End Face Seals with Diametral Tilt and Coning - Hydrodynamic Effects, ASLE preprint no. 79-LC-2A-1, presented at the ASME-ASLE Lubrication Conf., Oct. 1979.

8. Etsion, I.: Squeeze Effects in Radial Face Seals. Jour. of Lub. Tech., Trans. ASME, Vol. 102, No. 2, April 1980, pp. 145-152.

9. Banergee, B. N.; and Burton, R. A.: Experimental Studies on Thermoelastic Effects in Hydrodynamically Lubricated Face Seals. Journal of Lub. Tech., Trans. ASME, vol. 101, no. 3, July 1979, pp. 275-282.

10. Matt, R. J.: High Temperature Metal Bellows Seals for Aircraft and Missile Accessories. J. Engrg. for Industry, Trans. ASME, vol. 85, Aug. 1963, pp. 281-288.

11. Hudelson, J. C.: Dynamic Instability of Undamped Bellows Face Seals in Cryogenic Liquid. ASLE Trans., vol. 9, no. 4, Oct. 1966, pp. 381-390.

12. Storm, T. N.; Ludwig, L. P.; and Hudelson, J. C.: Vibration of Shaft Face Seals and Stabilizing Effect of Viscous and Friction Damping. NASA TN D-5161, April 1969.

13. Kaneta, M.; Fukahori, M.; and Hirano, F.: Dynamic Characteristics of Face Seals. Proc. 8th Int. Conf. on Fluid Sealing, BHRA, Sept. 1978, paper A2.

14. Etsion, I.; and Burton, R. A.: Observation of Self Excited Wobble in Face Seals. Journal of Lub. Tech., Trans. ASME, vol. 101, no. 4, Oct. 1979, pp. 526-528.

15. Haardt, R.; and Godet, M.: Axial Vibration of a Misaligned Radial Face Seal Under a Constant Closure Force. ASLE Trans., vol. 18, no. 1, Jan. 1975, pp. 56-61.

16. Zorowski, C. F.; and Hill, H. H.: Post Mechanical Separation in Elastically Supported Rotary Face Seals. ASLE Trans., vol. 14, no. 1, Jan. 1971, pp. 75-80.

17. Chaing, T.; and Cheng, H. S.: An Analysis of Flexible Seal Ring Vibrations. ASLE Trans., vol. 11, no. 3, July 1968, pp. 204-215.

18. Griskin, E.N.: The Effect of Dynamics on Fluid Flow in a Face Seal. Proc. 7th Int. Conf. on Fluid Sealing, BHRA, Sept. 1975, Paper B2.

19. Kupperman, D. S.: Dynamic Tracking of Noncontacting Face Seals. ASLE Trans., vol. 18, no. 4, Oct. 1975, pp. 306-311

20. Shapiro, W.; and Colsher, R.: Steady State and Dynamic Analysis of a Jet Engine, Gas-Lubricated Shaft Seal. ASLE Trans., vol. 17, no. 3, July 1974, pp. 190-200.

21. Etsion, I.; and Dan, Y.: An Analysis of Mechanical Face Seal Vibrations. ASME Paper 80-C2/Lub-8 to be presented at the ASLE-ASME Lubrication Conference, Aug. 1980.

22. Etsion, I.: Dynamic Response to Rotating-Seat Runout in Non-Contacting Face Seals. NASA TM-84190, April 1980.

23. Etsion, I.: The Accuracy of the Narrow Seal Approximation in Analyzing Radial Face Seals. ASLE Trans., vol. 23, no. 2, April 1980, pp. 208-216.

24. Metcalfe, R.: Dynamic Whirl in Well Aligned, Liquid Lubricated End Face Seals with Hydrostatic Tilt Instability. ASLE Preprint 80-LC-1B-1 to be presented at the ASME-ASLE Lubrication Conf., Aug. 1980.

TABLE I. - CHARACTERISTICS OF REPRESENTATIVE TEST CASES, $R_i = 0.9$

Case number	$(r_g/r_{sp})^2 m^* \omega^2 / K^*$	$\beta^* r_o / C_o$	$(r_m/r_{sp})^2 (p_o - p_i) \times r_o^2 / K^* C_o$	$M_e / S r_o^3$
1	32	10	90.25	0
2	21.95	10	90.25	0
3	8	10	90.25	0
4	8	10	90.25	0.01
5	8	2	90.25	0
6	8	50	90.25	0
7	8	100	90.25	0
8	32	10	361	0
9	32	10	902.5	0
10	32	10	3610	0

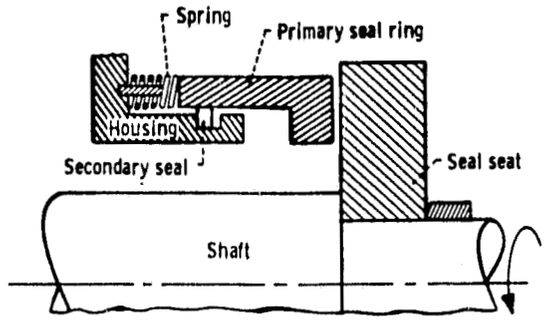

Figure 1. - Schematic of a radial face seal.

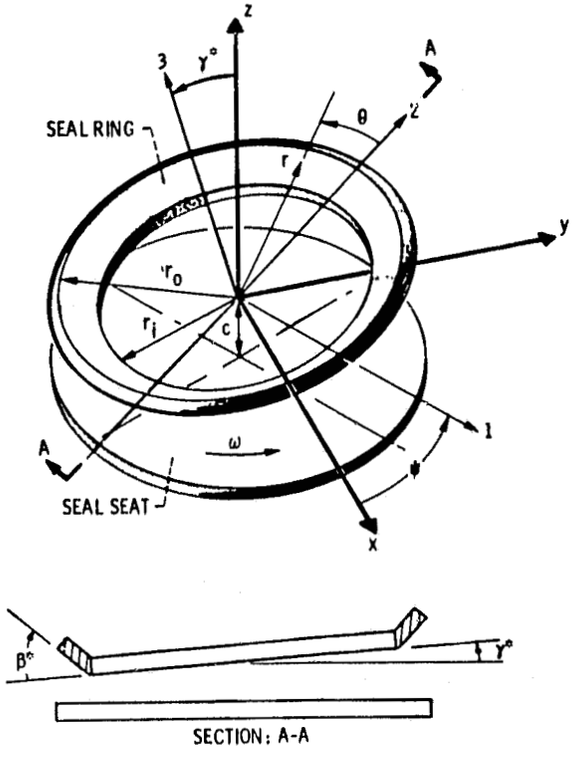

Figure 2. - Seal model and coordinates systems.

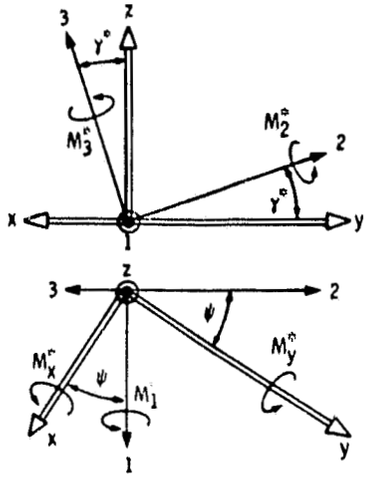

Figure 3. - Orientation of rotating cooridinate system 123 in inertial reference xyz.

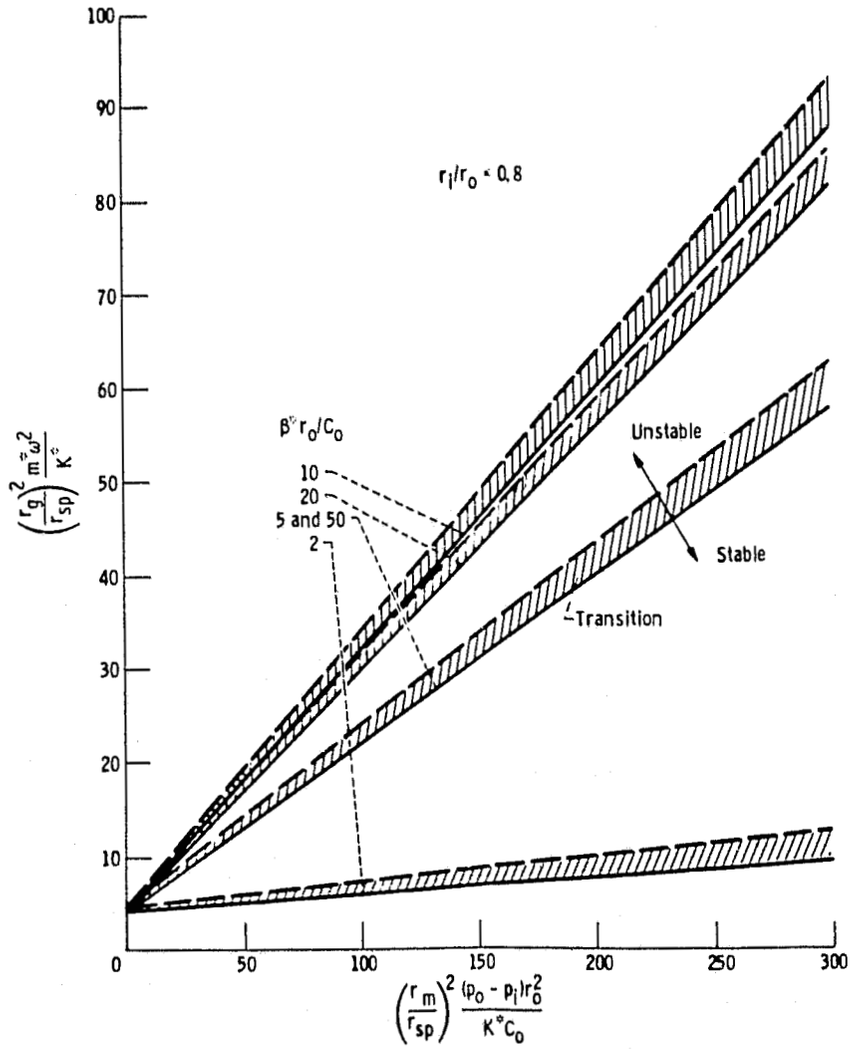

Figure 4. - Stability maps for seals of radius ratio $R_i = 0.8$.

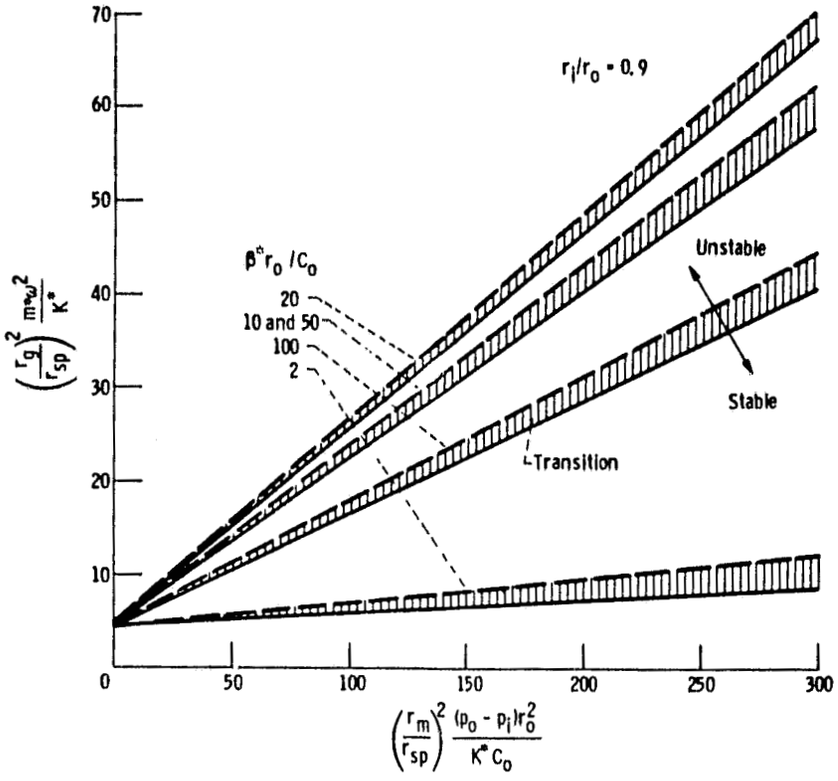

Figure 5. - Stability maps for seals of radius ratio $R_i = 0.9$.

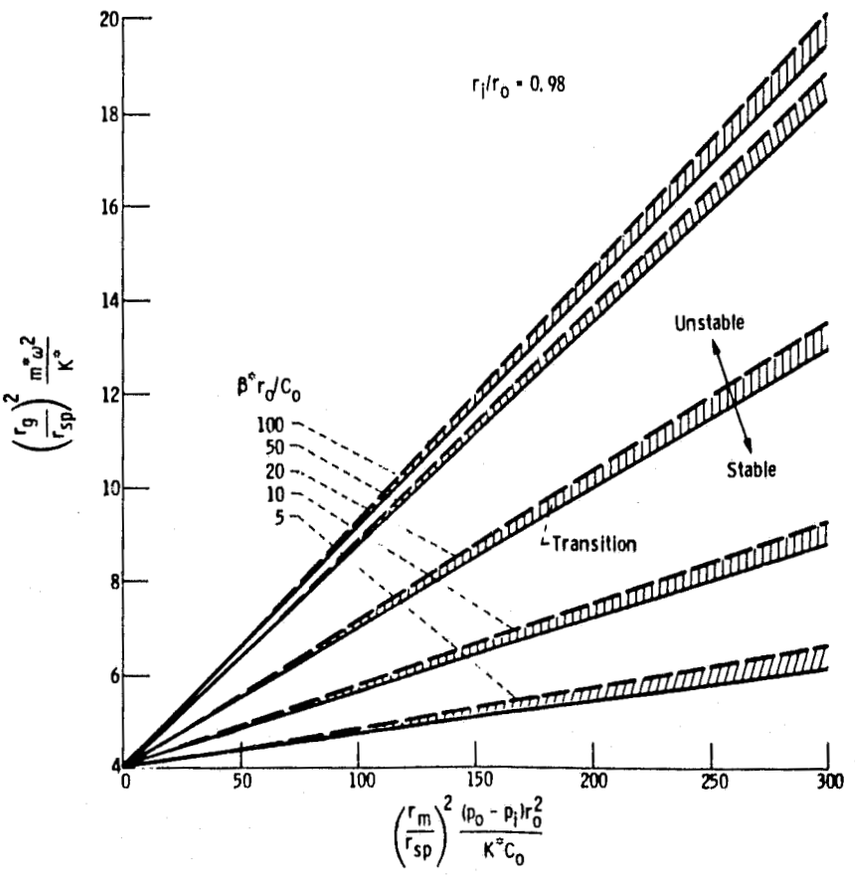

Figure 6. - Stability maps for seals of radius ratio $R_i = 0.98$.

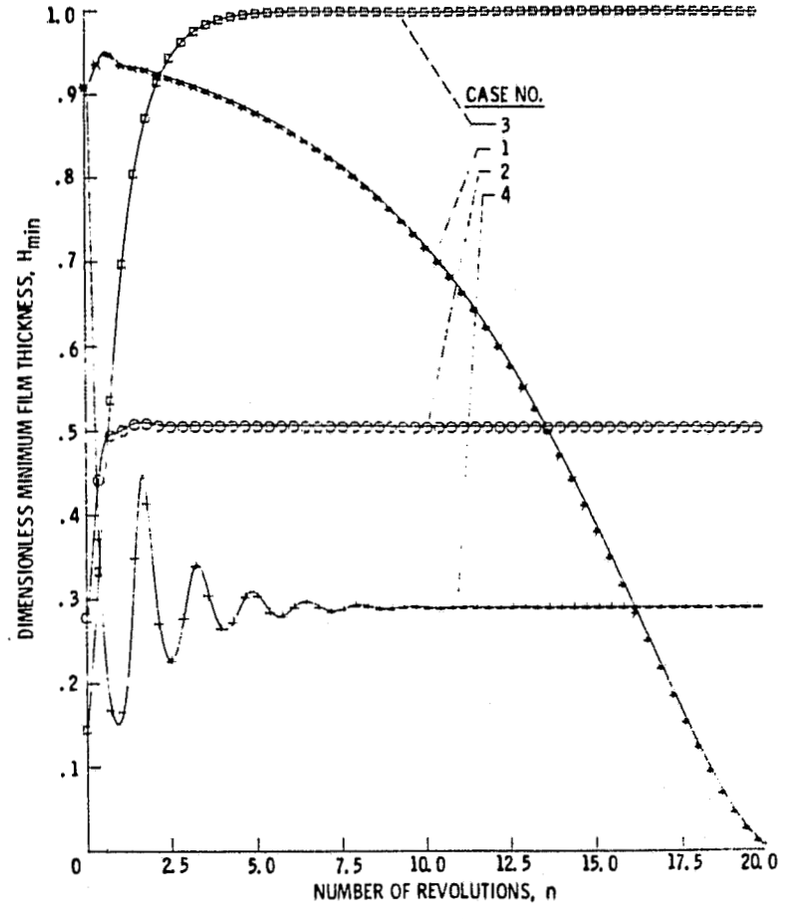

Figure 7. - Effect of the parameter $(r_g/r_{sp})^2 m^* \omega^2 / K^*$ on seal stability, $R_j = 0.9$.

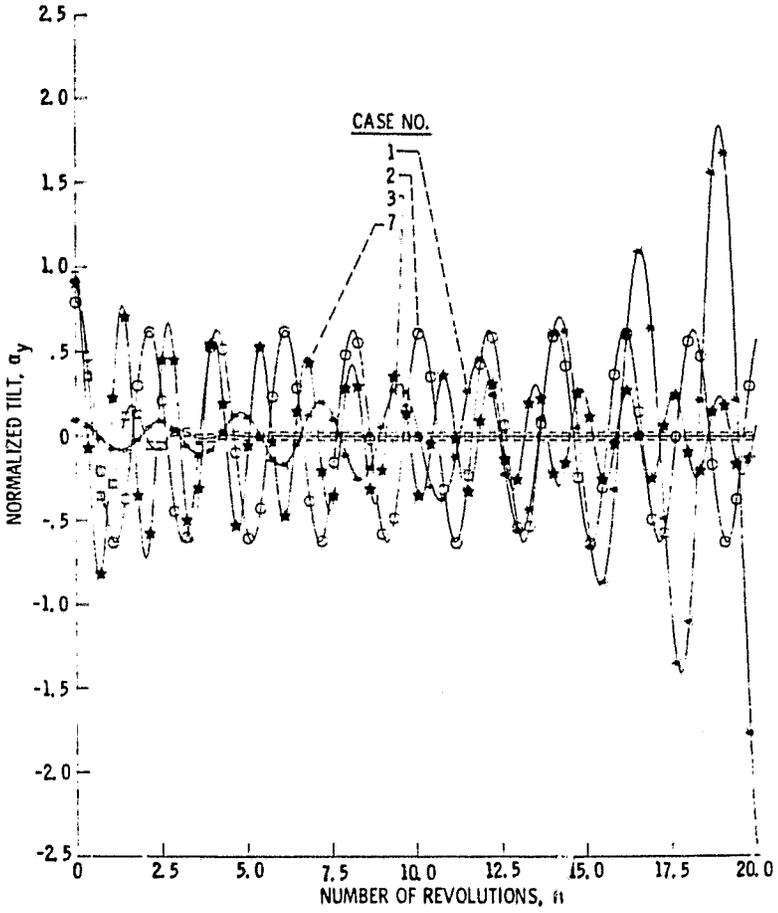

Figure 8. - Variation of normalized tilt with time for seals operating at various stability modes, $R_j = 0.9$.

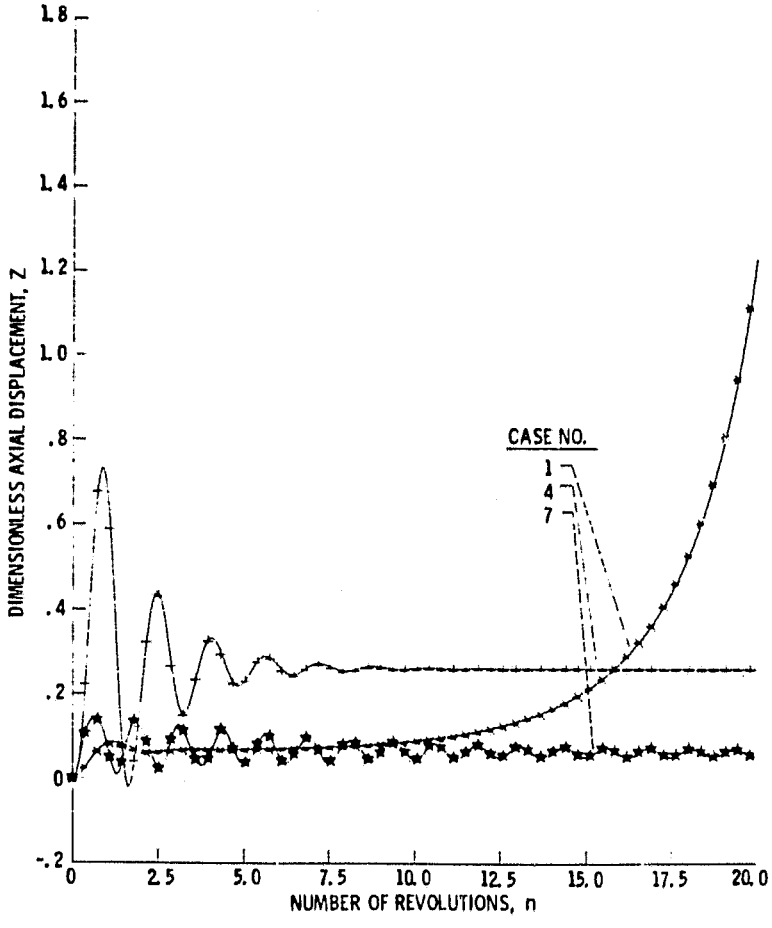

Figure 9. - Variation of dimensionless axial displacement with time for seals operating at various stability modes, $R_i = 0.9$.

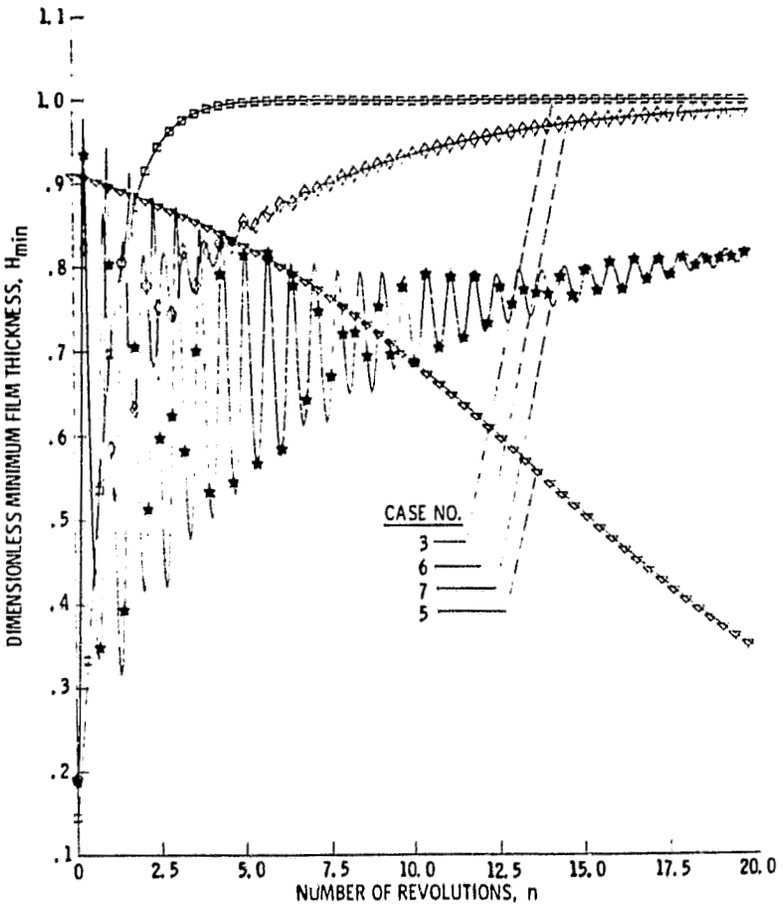

Figure 10. - Effect of the parameter $\beta^{*}r_o/C_o$ on seal stability, $R_j = 0.9$.

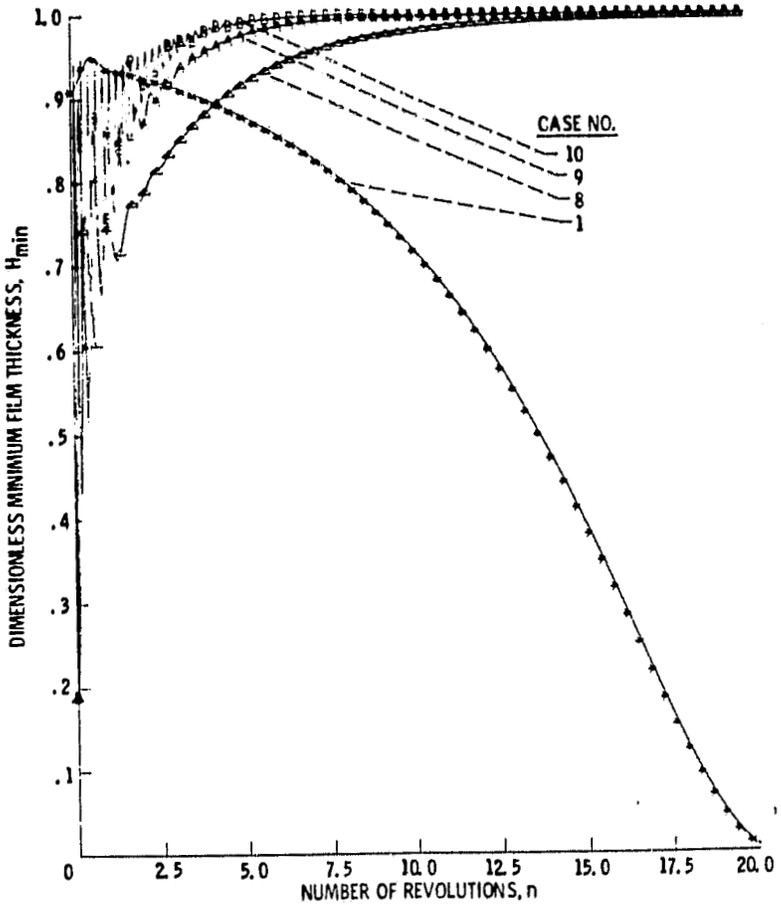

Figure 11. - Effect of the parameter $(r_m/r_{sp})^2(p_o-p_i)r_o^2/K^*C_o$ on seal stability, $R_i = 0.9$.